

Supplementary Information for  
**Breaking the Upper Bound of Siloxane Uptake:  
Metal-Organic Frameworks as an Adsorbent  
Platform**

Ezgi Gulcay-Ozcan  <sup>†a</sup>, Paul Iacomi  <sup>†a</sup>, Youngsang Ko<sup>b</sup>, Jong-San Chang<sup>b</sup>, Guillaume Rioland<sup>c</sup>, Sabine Devautour-Vinot  <sup>a</sup>, and Guillaume Maurin  <sup>a</sup>

<sup>†</sup> These authors contributed equally

\* E-Mail: [guillaume.maurin1@umontpellier.fr](mailto:guillaume.maurin1@umontpellier.fr)

<sup>a</sup>ICGM, Univ. Montpellier, CNRS, ENSCM, F-34095 Montpellier, France

<sup>b</sup>Research Group for Nanocatalyst (RGN) and Convergent Center for Chemical Process (CCP), Korea Research Institute of Chemical Technology (KRICT), Gajeong-ro 141, Yuseong-gu, Daejeon 34114, South Korea

<sup>c</sup>Centre National d'Etudes Spatiales, DSO/AQ/LE, 18 Avenue Edouard Belin, 31401 Toulouse, Cedex 09, France

## Contents

<b>1</b>	<b>Computational details</b>	<b>S3</b>
1.1	Force field parameters for D4	S3
1.2	Screening dataset	S4
1.3	Radial distribution functions for D4/PCN-777	S9
<b>2</b>	<b>MOF samples</b>	<b>S9</b>
2.1	MIL-101(Cr)	S9
2.2	DUT-4	S9
2.3	PCN-777	S9
<b>3</b>	<b>D4 sorption experiments</b>	<b>S12</b>
3.1	D4 benchmarking with known MOFs	S12
3.2	Isosteric heat of sorption of D4	S12
	<b>References</b>	<b>S13</b>

## 1. Computational details

**1.1. Force field parameters for D4.** D4 was modelled as a semi-flexible molecule with an all-atom atomistic model. All intramolecular bonds, angles, dihedrals, and cross terms parameters for methyl groups were taken from the consistent-valence force field (CVFF) reminded below.<sup>S1</sup>

### Harmonic Bond

$$U = \frac{1}{2}p_0(r - p_1)^2 \quad [S1]$$

where  $p_0/\kappa_B$  in units  $\text{K}/\text{\AA}^2$ ,  $p_1$  in  $\text{\AA}$ .

Table S1: D4 bonding potential parameters.

Pseudo atom	Type of bond	$p_0/\kappa_B$ ( $\text{K}/\text{\AA}^2$ )	$p_1$ ( $\text{\AA}$ )
Si-O	RIGID_BOND	-	-
Si-C	HARMONIC_BOND	286248.126	1.809
C3-H	HARMONIC_BOND	409668.576	1.105

### Harmonic Bend

$$U = \frac{1}{2}p_0(\theta_{ijk} - p_1)^2 \quad [S2]$$

where  $p_0/\kappa_B$  in units  $\text{K}/\text{rad}^2$ ,  $p_1$  in degree.

Table S2: D4 bending potential parameters.

Pseudo atom	Type of angle	$p_0/\kappa_B$ ( $\text{K}/\text{rad}^2$ )	$p_1$ ( $^\circ$ )
Si-C-H	HARMONIC_BEND	41614.223	112.3
C-Si-C	HARMONIC_BEND	53400.911	113.5
C-Si-O	HARMONIC_BEND	53040.094	117.3
H-C-H	HARMONIC_BEND	47507.567	106.4

### CVFF Dihedral

$$U = p_0(1 + \cos(p_1\phi_{ijk} - p_2))^2 \quad [S3]$$

where  $p_0/\kappa_B$  in units  $\text{K}$ ,  $p_2$  in degree.

Table S3: D4 dihedral potential parameters.

Pseudo atom	Type of torsion	$p_0/\kappa_B$ ( $\text{K}$ )	$p_1$ (multiplicity)	$p_2$ ( $^\circ$ )
H-C-Si-C	CVFF_DIHEDRAL	240.545	3	0
H-C-Si-O	CVFF_DIHEDRAL	-60.136	3	0
C-Si-O-Si	CVFF_DIHEDRAL	240.545	3	0

### CFF Bond Bond Cross

$$U = p_0(r - p_1)(r' - p_2) \quad [S4]$$

where  $p_0/\kappa_B$  in units  $\text{K}/\text{\AA}^2$ ,  $p_1$  and  $p_2$  in  $\text{\AA}$

Table S4: D4 cross-term bonding potential parameters.

Pseudo atom	Type of bond-bond	$p_0/\kappa_B$ ( $\text{K}/\text{\AA}^2$ )	$p_1$ ( $\text{\AA}$ )	$p_2$ ( $\text{\AA}$ )
Si-C-H	CFF_BOND_BOND_CROSS	14312.406	0	0
C-Si-C	CFF_BOND_BOND_CROSS	7336.612	0	0
C-Si-O	CFF_BOND_BOND_CROSS	25257.188	0	0

## CFF Bond Bend Cross

$$U = (\theta - p_0)[p_1(r - p_2) + p_3(r' - p_4)] \quad [S5]$$

where  $p_0$  in degrees,  $p_1$  and  $p_3$  in units K/Å/rad,  $p_2$  and  $p_4$  in Å.

**Table S5:** D4 cross-term bonding-bending potential parameters.

Pseudo atom	Type of bond-angle	$p_0$ (°)	$p_1$ (K/Å/rad)	$p_2$ (Å)	$p_3$ (K/Å/rad)	$p_4$ (Å)
Si-C-H	CFF_BOND_BEND_CROSS	0	14733.359	0	9742.06	0
C-Si-C	CFF_BOND_BEND_CROSS	0	781.770	0	0	0
C-Si-O	CFF_BOND_BEND_CROSS	0	11425.871	0	27061.27	0

## D4 LJ parameters and charges

The electronic potential (ESP) derived partial charges of D4 were computed by density functional theory (DFT) calculations with PBE (Perdew-Burke-Ernzerhof) functional<sup>S2</sup> and DNP (double numeric plus polarization) basis set<sup>S3</sup>, using DMol<sup>3</sup><sup>S4</sup> (Table S6).

**Table S6:** Charges and LJ parameters for all atoms of D4.

Pseudo atom	Charge (e <sup>-</sup> )	$\epsilon/\kappa_B$ (K)	$\sigma$ (Å)
Si	1.321	202.429	3.826
O	-0.763	30.213	3.118
C	-0.889	52.873	3.431
H	0.2032	22.156	2.571

## 1.2. Screening dataset. Material details.

**Table S7:** Details of the 29 MOFs added to the COREMOF database.

MOFs	Reference	MOFs	Reference
RAVWAO	S5	DUT-5	S6
RAVWES	S5	DUT-51-Zr	S7
RAVWIW	S5	DUT-67-Zr	S8
RAVWOC	S5	MIL-68(Al)	S9
RAVWUI	S5	Cr-soc-MOF-1	S10
RAVXAP	S5	MIP <sup>[4]</sup> -177	S11
RAVXET	S5	MIP-200	S12
RAVXIX	S5	Zr-IPA <sup>[5]</sup>	S13
MIL-125	S14	Ni-BPM <sup>[6]</sup>	S15
MOF-808-acetate	S14	Ni-BPP <sup>[7]</sup>	S15
MOF-808-formate	S14	Ni-TPM <sup>[8]</sup>	S15
NU <sup>[1]</sup> -1000	S14	Ni-TPP <sup>[9]</sup>	S15
UiO <sup>[2]</sup> -68	S14	Ni-MOF-74	S15
Zr6-AzoBDC <sup>[3]</sup>	S14	PCN <sup>[10]</sup> -224(Ni)	S16

[1]NU: Northwestern University; [2]UiO: University of Oslo;

[3]AzoBDC: azobenzenedicarboxylate;

[4]MIP: Material of the Institute of Porous Materials from Paris;

[5]IPA: isophatale; [6]BPM: biphenyl-meta;

[7]BPP: biphenyl-para; [8]TPM: triphenyl-meta;

[9]TPP: triphenyl-para; [10]PCN: Porous coordination network;

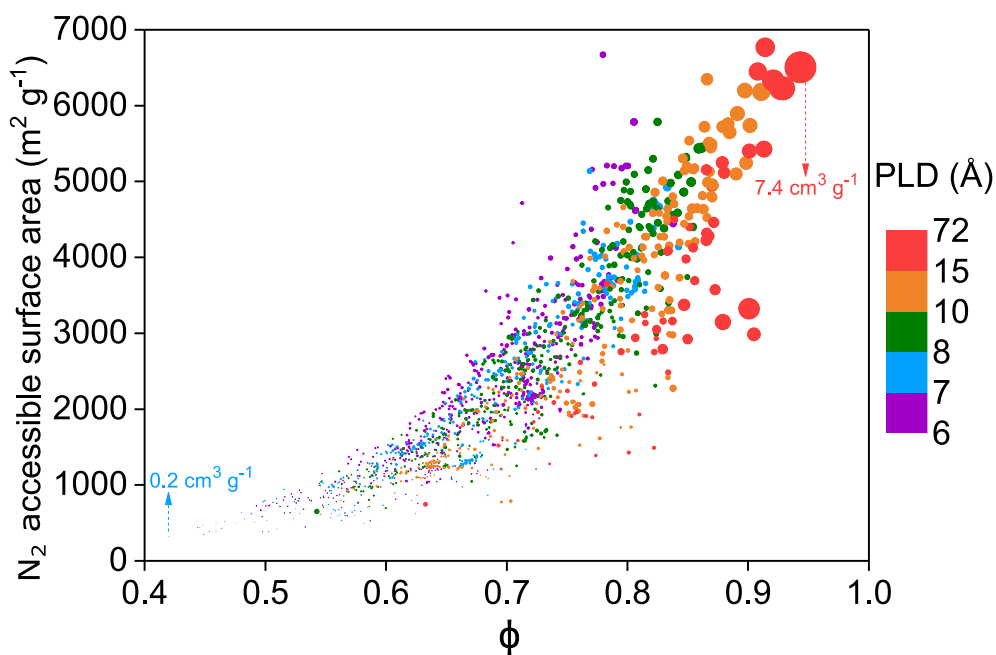


**Fig. S1:** Overview of the diversity of the MOF database with PLD > 6 Å in terms of void fractions,  $N_2$  accessible surface areas and PLDs. Data points are color coded by PLDs of MOFs. Pore volumes of all structures are represented by size.

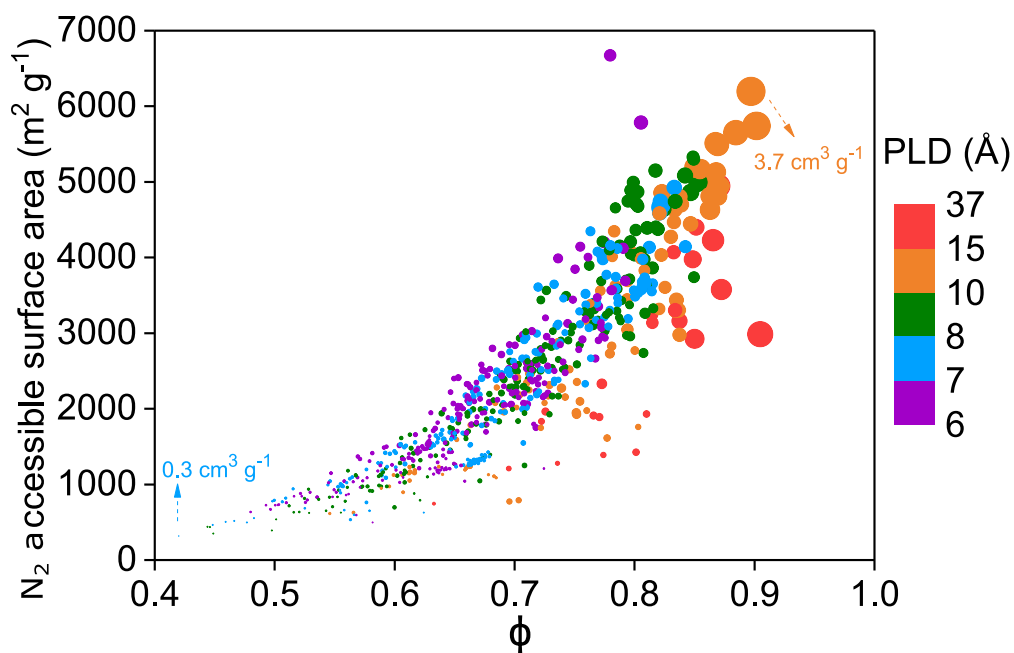


**Fig. S2:** Overview of the diversity of the hydrophobic MOFs database in terms of void fraction and  $N_2$  accessible surface areas. Data points are color coded by PLDs of MOFs. Pore volumes of all structures are represented by size.

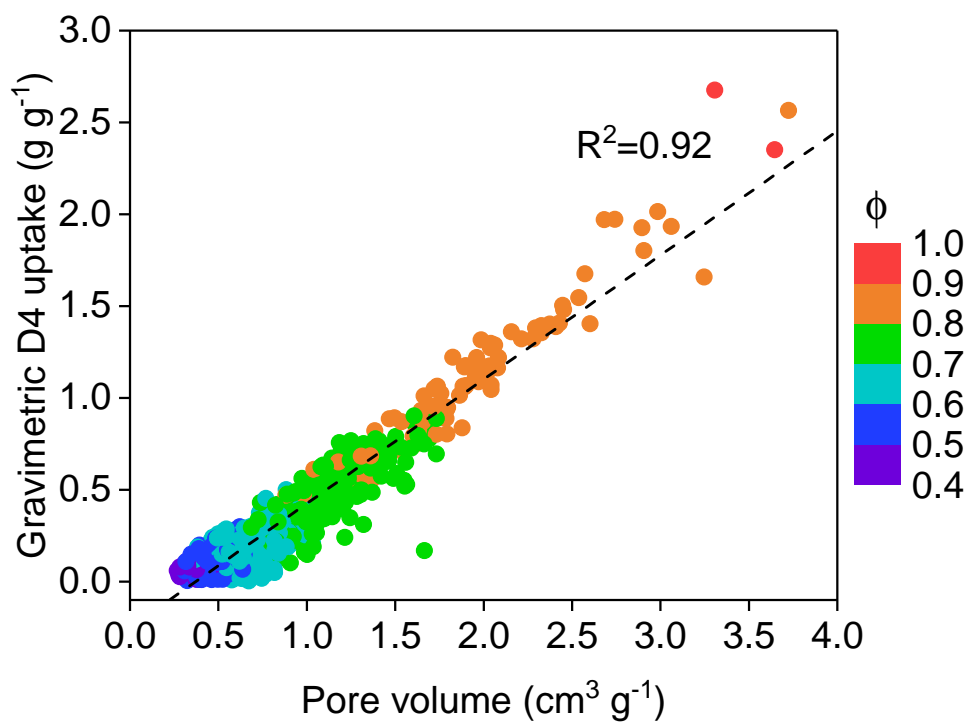


Fig. S3: The relation between the gravimetric D4 uptake of the 811 hydrophobic MOFs ( $\text{g g}^{-1}$ ) and their pore volumes ( $\text{cm}^3 \text{g}^{-1}$ ), color coded by void fraction of the MOFs.

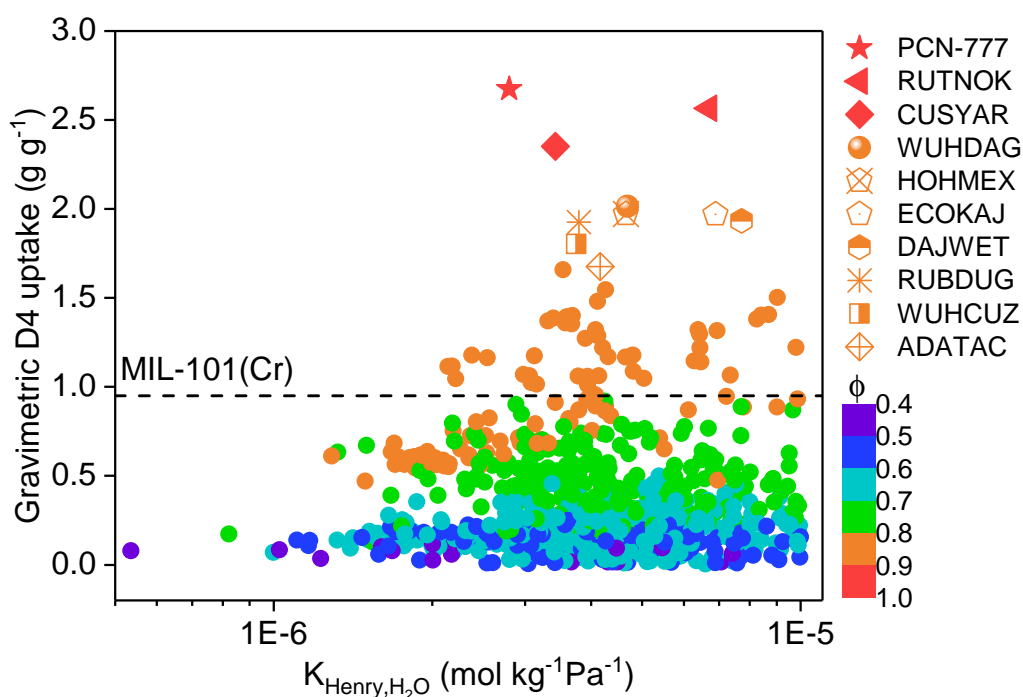
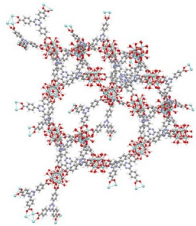
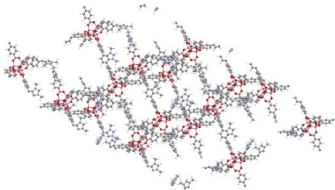
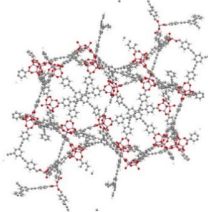
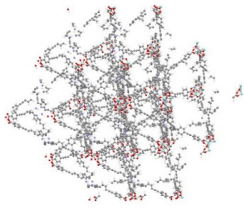
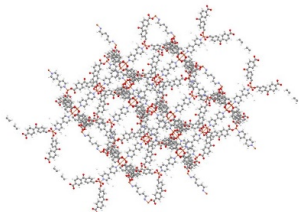
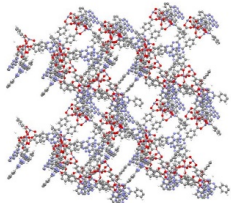


Fig. S4: Predicted D4 uptake performance at 298 K for the hydrophobic MOFs database plotted as a function of their computed Henry constant of water, color coded by void fraction,  $\phi$ . Top performing 10 candidates are represented by different symbols in the legend to the right.

Table S8: Structural details of the top promising 10 hydrophobic materials which exhibit the highest D4 uptake.

MOF	Details
<p><b>FOTNIN (PCN-777)</b></p> 	<p><b>Organic ligand:</b> 4,4',4'-s-triazine-2,4,6-triyl-tribenzoic acid  <b>Metal site:</b> Zr  <b>PLD:</b> 28.36 Å  <b>SA:</b> 2990 m<sup>2</sup> g<sup>-1</sup>  <b>Density:</b> 0.27 g cm<sup>-3</sup>  <b>PV:</b> 3.31 cm<sup>3</sup> g<sup>-1</sup>  <math>\phi</math>: 0.90  <b>Gravimetric D4 uptake:</b> 2.68 g g<sup>-1</sup>  <b>Volumetric D4 uptake:</b> 0.72 g cm<sup>-3</sup></p>
<p><b>RUTNOK (IRMOF-76)</b></p> 	<p><b>Organic ligand:</b> 4,7-bis(4-carboxylphenyl)-1,3-dimethylbenzimidazolium-tetrafluoroborate  <b>Metal site:</b> Zn  <b>PLD:</b> 14.65 Å  <b>SA:</b> 6200 m<sup>2</sup> g<sup>-1</sup>  <b>Density:</b> 0.24 g cm<sup>-3</sup>  <b>PV:</b> 3.72 cm<sup>3</sup> g<sup>-1</sup>  <math>\phi</math>: 0.90  <b>Gravimetric D4 uptake:</b> 2.57 g g<sup>-1</sup>  <b>Volumetric D4 uptake:</b> 0.62 g cm<sup>-3</sup></p>
<p><b>CUSYAR (MOF-210)</b></p> 	<p><b>Organic ligand:</b> biphenyl-4,4'-dicarboxylate  <b>Metal site:</b> Zn  <b>PLD:</b> 12.18 Å  <b>SA:</b> 5700 m<sup>2</sup> g<sup>-1</sup>  <b>Density:</b> 0.25 g cm<sup>-3</sup>  <b>PV:</b> 3.65 cm<sup>3</sup> g<sup>-1</sup>  <math>\phi</math>: 0.90  <b>Gravimetric D4 uptake:</b> 2.35 g g<sup>-1</sup>  <b>Volumetric D4 uptake:</b> 0.59 g cm<sup>-3</sup></p>
<p><b>WUHDAG (NU-1104)</b></p> 	<p><b>Organic ligand:</b> meso-tetrakis-(4-((phenyl)ethynyl)benzoate) porphyrin  <b>Metal site:</b> Zr  <b>PLD:</b> 10.50 Å  <b>SA:</b> 5500 m<sup>2</sup> g<sup>-1</sup>  <b>Density:</b> 0.29 g cm<sup>-3</sup>  <b>PV:</b> 2.99 cm<sup>3</sup> g<sup>-1</sup>  <math>\phi</math>: 0.87  <b>Gravimetric D4 uptake:</b> 2.01 g g<sup>-1</sup>  <b>Volumetric D4 uptake:</b> 0.58 g cm<sup>-3</sup></p>
<p><b>HOHMEX</b></p> 	<p><b>Organic ligand:</b> 4,4'-carbonyldibenzoato - (<math>\mu</math>2-4,4'-bipyridine)  <b>Metal site:</b> Cu  <b>PLD:</b> 14.89 Å  <b>SA:</b> 5000 m<sup>2</sup> g<sup>-1</sup>  <b>Density:</b> 0.32 g cm<sup>-3</sup>  <b>PV:</b> 2.74 cm<sup>3</sup> g<sup>-1</sup>  <math>\phi</math>: 0.87  <b>Gravimetric D4 uptake:</b> 1.97 g g<sup>-1</sup>  <b>Volumetric D4 uptake:</b> 0.63 g cm<sup>-3</sup></p>
<p><b>ECOKAJ</b></p> 	<p><b>Organic ligand:</b> s-heptazine tribenzoate  <b>Metal site:</b> Zn  <b>PLD:</b> 17.58 Å  <b>SA:</b> 3600 m<sup>2</sup> g<sup>-1</sup>  <b>Density:</b> 0.33 g cm<sup>-3</sup>  <b>PV:</b> 2.68 cm<sup>3</sup> g<sup>-1</sup>  <math>\phi</math>: 0.87  <b>Gravimetric D4 uptake:</b> 1.97 g g<sup>-1</sup>  <b>Volumetric D4 uptake:</b> 0.65 g cm<sup>-3</sup></p>

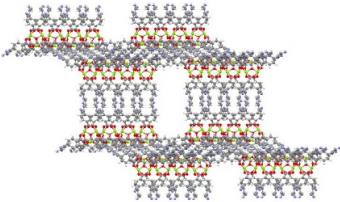
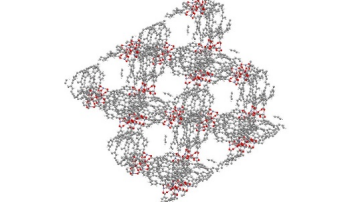
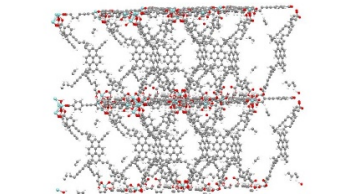
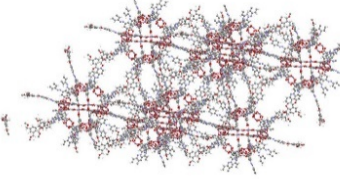
<p><b>DAJWET</b></p> 	<p><b>Organic ligand:</b> tetrakis (4-carboxylatophenyl) porphyrin  <b>Metal site:</b> Mg  <b>PLD:</b> 26.59 Å  <b>SA:</b> 5000 m<sup>2</sup> g<sup>-1</sup>  <b>Density:</b> 0.28 g cm<sup>-3</sup>  <b>PV:</b> 3.06 cm<sup>3</sup> g<sup>-1</sup>  <math>\phi</math>: 0.87  <b>Gravimetric D4 uptake:</b> 1.93 g g<sup>-1</sup>  <b>Volumetric D4 uptake:</b> 0.54 g cm<sup>-3</sup></p>
<p><b>RUBDUP</b></p> 	<p><b>Organic ligand:</b> phenylene ethynylene macrocycle  <b>Metal site:</b> Zn  <b>PLD:</b> 19.25 Å  <b>SA:</b> 4200 m<sup>2</sup> g<sup>-1</sup>  <b>Density:</b> 0.30 g cm<sup>-3</sup>  <b>PV:</b> 2.90 cm<sup>3</sup> g<sup>-1</sup>  <math>\phi</math>: 0.87  <b>Gravimetric D4 uptake:</b> 1.93 g g<sup>-1</sup>  <b>Volumetric D4 uptake:</b> 0.58 g cm<sup>-3</sup></p>
<p><b>WUHCUZ (NU-1103)</b></p> 	<p><b>Organic ligand:</b> 4,4',4'''-((pyrene-1,3,6,8 tetrayltetrakis(benzene-4,1-diy)) tetrakis(ethyne-2,1 diy))tetrabenzoate  <b>Metal site:</b> Zr  <b>PLD:</b> 12.21 Å  <b>SA:</b> 5500 m<sup>2</sup> g<sup>-1</sup>  <b>Density:</b> 0.30 g cm<sup>-3</sup>  <b>PV:</b> 2.91 cm<sup>3</sup> g<sup>-1</sup>  <math>\phi</math>: 0.87  <b>Gravimetric D4 uptake:</b> 1.80 g g<sup>-1</sup>  <b>Volumetric D4 uptake:</b> 0.54 g cm<sup>-3</sup></p>
<p><b>ADATAC</b></p> 	<p><b>Organic ligand:</b> 5,5',5''-(4,4',4''-[1,3,5-phenyltris(methoxy)] tris-phenylazo) tris-isophthalic acid  <b>Metal site:</b> Zn  <b>PLD:</b> 10.28 Å  <b>SA:</b> 5130 m<sup>2</sup> g<sup>-1</sup>  <b>Density:</b> 0.34 g cm<sup>-3</sup>  <b>PV:</b> 2.57 cm<sup>3</sup> g<sup>-1</sup>  <math>\phi</math>: 0.87  <b>Gravimetric D4 uptake:</b> 1.68 g g<sup>-1</sup>  <b>Volumetric D4 uptake:</b> 0.57 g cm<sup>-3</sup></p>

Table S9: Discussion on MOF selection.

Refcode	Given name	Observation	Reference
RUTNOK	IRMOF-76	Synthesis results in interpenetrated nets and the materials cannot be activated.	S17
CUSYAR	MOF-210	Material requires supercritical CO <sub>2</sub> activation, otherwise it collapses upon solvent removal.	S18
WUHDAG	NU-1104	Complex tetratopic porphyrin linker, difficult to synthesize and scale, and supercritical CO <sub>2</sub> activation is required.	S19
HOHMEX	SNU-6	The difference between our predicted and as-synthesized pore volume for this MOF was found as 2.74 vs 1.05 cm <sup>3</sup> g <sup>-1</sup> , respectively. Moreover, air exposure was reported to reduce significantly its H <sub>2</sub> capacity, highlighting water instability.	S20
WIHCUZ	NU-1103	Complex tetratopic conjugated pyrene core linker, difficult to synthesize and scale and supercritical CO <sub>2</sub> activation is required.	S19



### 1.3. Radial distribution functions for D4/PCN-777. Calculated at specified loading.

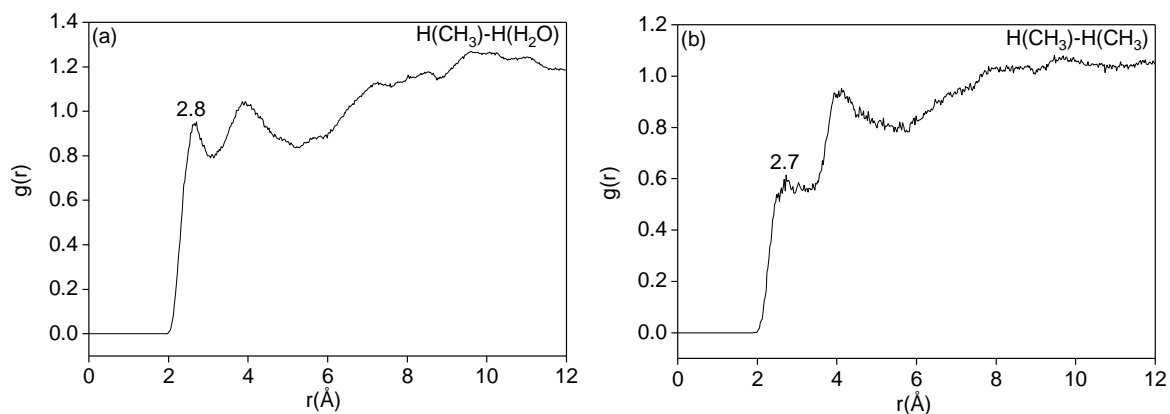


Fig. S5: All-atom averaged radial distribution functions between (a) H atom from CH<sub>3</sub> group of D4 molecules and H atom from coordinated water of the framework at 10% total loading and (b) H atom from CH<sub>3</sub> groups of D4 at 100% loading.

## 2. MOF samples

**2.1. MIL-101(Cr).** The benchmark MIL-101(Cr) sample was taken from a previous work <sup>S21</sup>, with all textural characteristics as stated in reference.

**2.2. DUT-4.** DUT-4 was purchased from Materials Center (TU Dresden, Germany).

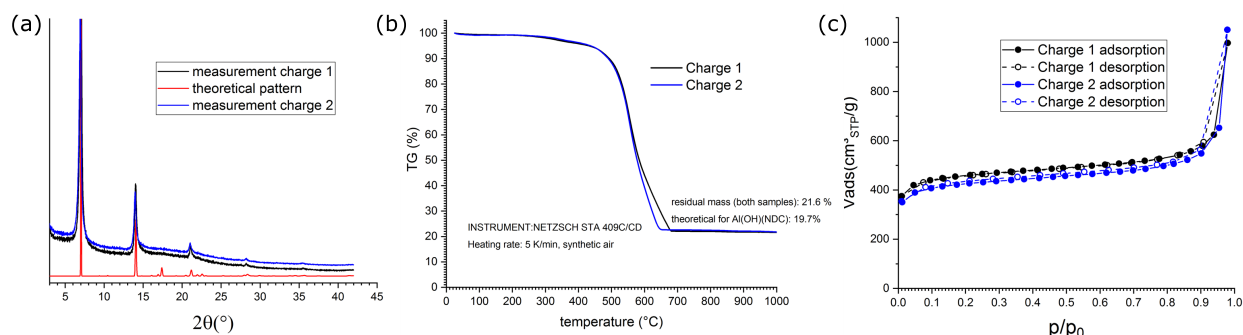


Fig. S6: Characterization of the DUT-4 sample, in duplicates as black and blue: (a) PXRD, alongside simulated pattern in red (b) TGA curves and (c) N<sub>2</sub> physisorption isotherms at 77 K.

### 2.3. PCN-777. Synthesis

To synthesize the PCN-777, ZrOCl<sub>2</sub> · 8 H<sub>2</sub>O (1.08 g, 3.351 mmol) and 4,4',4''-s-Triazine-2,4,6-triyl-tribenzoic acid (0.270 g, 0.612 mmol) were put into 36 ml N,N-Diethylformamide (DEF) in a 100 ml Teflon-lined autoclave reactor, alongside an amount of trifluoroacetic acid (1.8 ml) to form a reaction solution. After sonicating the reaction solution at room temperature for 10 min, the reactor was transferred to a convection oven followed by heating at 423 K for 12 h. The PCN-777 crystalline solid was recovered by filtration after purification with 100 ml N,N-Dimethylformamide (DMF) and acetone for 3 h at room temperature. The collected crystalline solid was dried at 393 K for 12 h.

## Characterisation

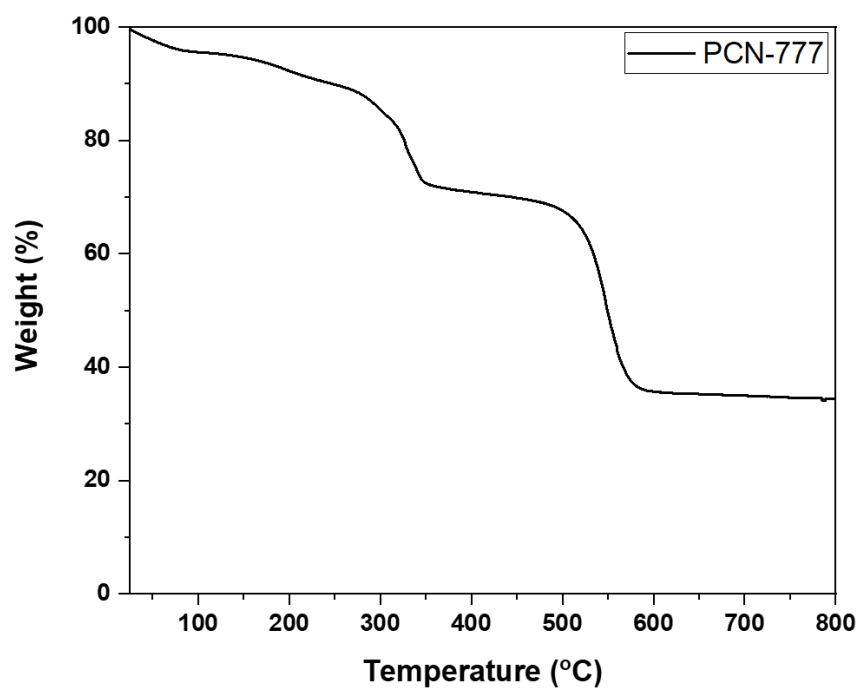


Fig. S7: Thermogravimetric curve recorded on as-synthesised PCN-777.

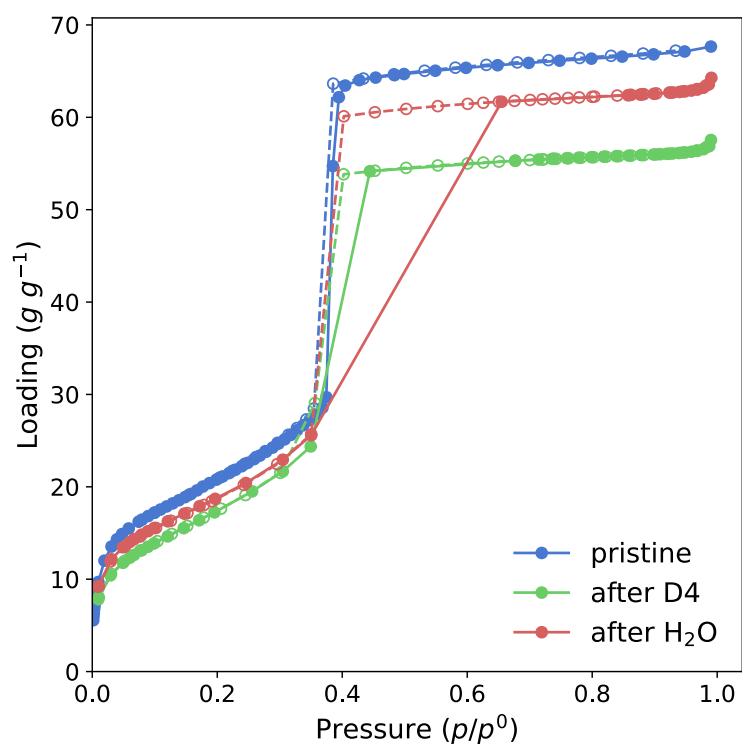


Fig. S8: Nitrogen sorption isotherms at 77 K for the pristine PCN-777, alongside with those measured on samples after D4 and water sorption.

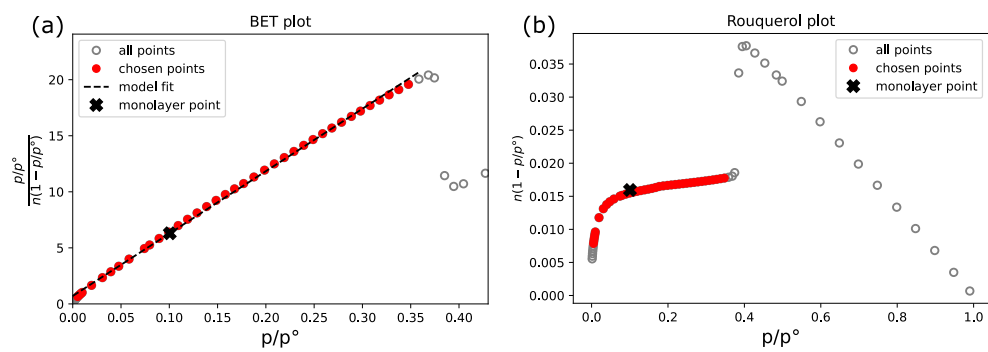
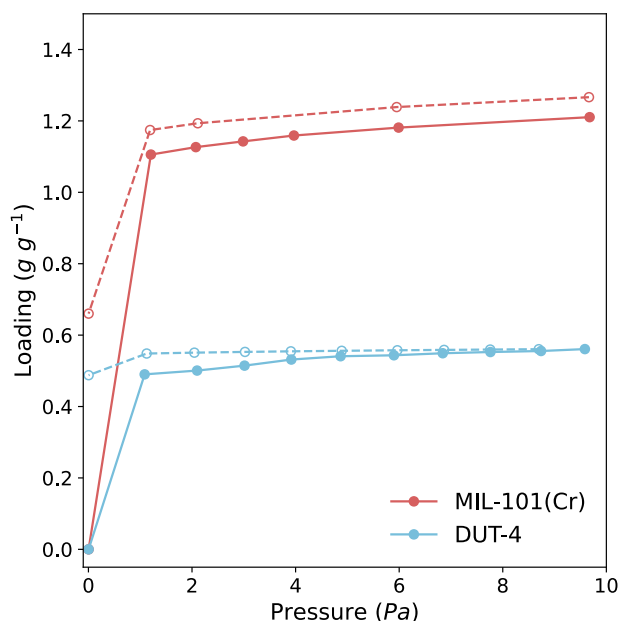


Fig. S9: BET and Rouquerol plots displaying selection of applicable isotherm points for the pristine PCN-777 isotherm.

### 3. D4 sorption experiments

**3.1. D4 benchmarking with known MOFs.** Isotherms were recorded on benchmark materials MIL-101(Cr) and DUT-4 using the same methodology detailed in the main manuscript.



**Fig. S10:** D4 isotherms recorded on samples of MIL-101(Cr) (red) and DUT-4 (blue), used to validate our computational methodology for predicting total D4 capacity. Note the different desorption behavior (open symbols) of the two materials under secondary vacuum: partial desorption for MIL-101(Cr) and no desorption for DUT-4.

**3.2. Isostatic heat of sorption of D4.** A further isotherm was recorded at 313 K (40 °C) to allow for the calculation of the isosteric heat of adsorption through the Clausius-Clapeyron equation, as depicted in Fig. S11.

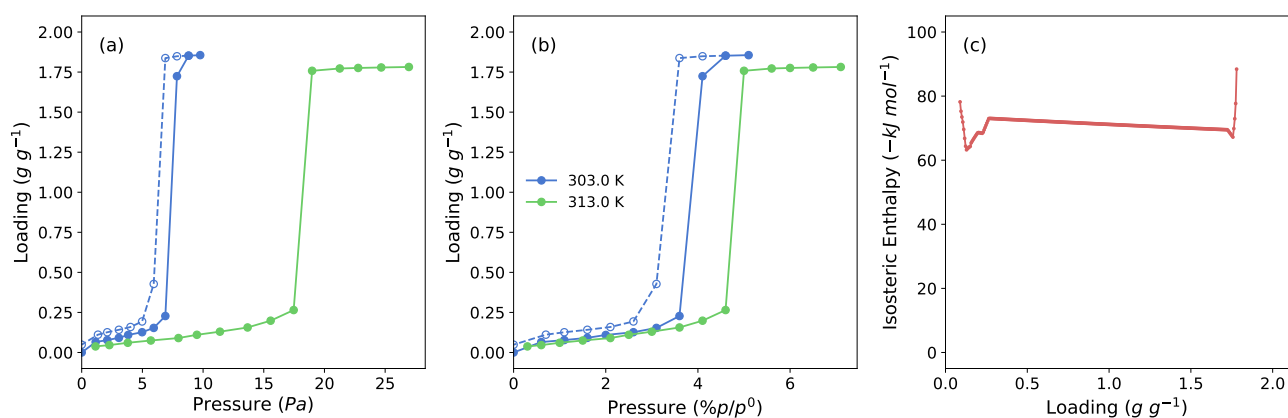


**Fig. S11:** D4 sorption isotherms on PCN-777 recorded at 303 K (blue) and at 313 K (green) in an absolute (a) and relative (b) pressure scale. (c) The calculated isosteric heat of adsorption as a function of D4 uptake.

## References

- (S1) Dauber-Osguthorpe, P.; Roberts, V.A.; Osguthorpe, D.J.; Wolff, J.; Genest, M.; and Hagler, A.T. "Structure and energetics of ligand binding to proteins: Escherichia coli dihydrofolate Reductase-Trimethoprim, a Drug-Receptor system." *Proteins: Struct, Funct, Bioinf*, 1988. **4**(1):31–47
- (S2) Perdew, J.P.; Burke, K.; and Ernzerhof, M. "Generalized Gradient Approximation Made Simple." *Physical Review Letters*, 1996. **77**(18):3865–3868. doi:10.1103/PhysRevLett.77.3865
- (S3) Hehre, W.J.; Ditchfield, R.; and Pople, J.A. "Self-consistent molecular orbital methods. XII. Further extensions of gaussian-type basis sets for use in molecular orbital studies of organic molecules." *J Chem Phys*, 1972. **56**(5):2257–2261
- (S4) Delley, B. "An All-electron numerical method for solving the local density functional for polyatomic molecules." *J Chem Phys*, 1990. **92**(1):508–517
- (S5) Gulcay, E. and Erucar, I. "Biocompatible MOFs for storage and separation of O<sub>2</sub>: A molecular simulation study." *Ind Eng Chem Res*, 2019. **58**(8):3225–3237
- (S6) Senkovska, I.; Hoffmann, F.; Fröba, M.; Getzschmann, J.; Böhlmann, W.; and Kaskel, S. "New highly porous aluminium based metal-organic frameworks: Al(OH)(ndc) (ndc=2,6-naphthalene dicarboxylate) and Al(OH)(bpd) (bpd=4,4'-biphenyl dicarboxylate)." *Microporous and Mesoporous Materials*, 2009. **122**(1-3):93–98. doi:10.1016/j.micromeso.2009.02.020
- (S7) Bon, V.; Senkovskyy, V.; Senkovska, I.; and Kaskel, S. "Zr(IV) and Hf(IV) based metal-organic frameworks with reo-topology." *Chem Commun*, 2012. **48**(67):8407. doi:10.1039/c2cc34246d
- (S8) Bon, V.; Senkovska, I.; Baburin, I.A.; and Kaskel, S. "Zr- and Hf-Based Metal-Organic Frameworks: Tracking Down the Polymorphism." *Crystal Growth & Design*, 2013. **13**(3):1231–1237. doi:10.1021/cg301691d
- (S9) Yang, Q.; Vaesen, S.; Vishnuvarthan, M.; Ragon, F.; Serre, C.; Vimont, A.; Daturi, M.; De Weireld, G.; and Maurin, G. "Probing the adsorption performance of the hybrid porous MIL-68(Al): A synergic combination of experimental and modelling tools." *Journal of Materials Chemistry*, 2012. **22**(20):10210. doi:10.1039/c2jm15609a
- (S10) Nandi, S.; Aggarwal, H.; Wahiduzzaman, M.; Belmabkhout, Y.; Maurin, G.; Eddaoudi, M.; and Devautour-Vinot, S. "Revisiting the water sorption isotherm of MOF using electrical measurements." *Chem Commun*, 2019. **55**(88):13251–13254
- (S11) Wang, S.; Kitao, T.; Guillou, N.; Wahiduzzaman, M.; Martineau-Corcus, C.; Nouar, F.; Tissot, A.; Binet, L.; Ramsahye, N.; Devautour-Vinot, S.; Kitagawa, S.; Seki, S.; Tsutsui, Y.; Briois, V.; Steunou, N.; Maurin, G.; Uemura, T.; and Serre, C. "A phase transformable ultrastable titanium-carboxylate framework for photoconduction." *Nature Communications*, 2018. **9**(1). doi:10.1038/s41467-018-04034-w
- (S12) Wang, S.; Lee, J.S.; Wahiduzzaman, M.; Park, J.; Muschi, M.; Martineau-Corcus, C.; Tissot, A.; Cho, K.H.; Marrot, J.; Shepard, W.; Maurin, G.; Chang, J.S.; and Serre, C. "A robust large-pore zirconium carboxylate metal-organic framework for energy-efficient water-sorption-driven refrigeration." *Nat Energy*, 2018. **3**(11):985–993. doi:10.1038/s41560-018-0261-6
- (S13) Wang, S.; Chen, L.; Wahiduzzaman, M.; Tissot, A.; Zhou, L.; Ibarra, I.A.; Gutiérrez-Alejandre, A.; Lee, J.S.; Chang, J.S.; Liu, Z.; Marrot, J.; Shepard, W.; Maurin, G.; Xu, Q.; and Serre, C. "A Mesoporous Zirconium-Isophthalate Multifunctional Platform." *Matter*, 2020. p. S2590238520305634. doi:10.1016/j.matt.2020.10.009
- (S14) Soares, C.V.; Leitão, A.; and Maurin, G. "Computational evaluation of the chemical warfare agents capture performances of robust MOFs." *Microporous Mesoporous Mater*, 2019. **280**:97–104. doi:10.1016/j.micromeso.2019.01.046
- (S15) Zheng, J.; Barpaga, D.; Trump, B.A.; Shetty, M.; Fan, Y.; Bhattacharya, P.; Jenks, J.J.; Su, C.Y.; Brown, C.M.; Maurin, G.; McGrail, B.P.; and Motkuri, R.K. "Molecular Insight into Fluorocarbon Adsorption in Pore Expanded Metal-Organic Framework Analogs." *J Am Chem Soc*, 2020. **142**(6):3002–3012. doi:10.1021/jacs.9b11963
- (S16) Feng, D.; Chung, W.C.; Wei, Z.; Gu, Z.Y.; Jiang, H.L.; Chen, Y.P.; Darendsbourg, D.J.; and Zhou, H.C. "Construction of Ultrastable Porphyrin Zr Metal-Organic Frameworks through Linker Elimination." *J Am Chem Soc*, 2013. **135**(45):17105–17110. doi:10.1021/ja408084j
- (S17) Oisaki, K.; Li, Q.; Furukawa, H.; Czaja, A.U.; and Yaghi, O.M. "A Metal-organic framework with covalently bound organometallic complexes." *J Am Chem Soc*, 2010. **132**(27):9262–9264. doi:10.1021/ja103016y
- (S18) Furukawa, H.; Ko, N.; Go, Y.B.; Aratani, N.; Choi, S.B.; Choi, E.; Yazaydin, A.O.; Snurr, R.Q.; O'Keeffe, M.; Kim, J.; and Yaghi, O.M. "Ultrahigh Porosity in Metal-Organic Frameworks." *Science*, 2010. **329**(5990):424–428. doi:10.1126/science.1192160
- (S19) Wang, T.C.; Bury, W.; Gómez-Gualdrón, D.A.; Vermeulen, N.A.; Mondloch, J.E.; Deria, P.; Zhang, K.; Moghadam, P.Z.; Sarjeant, A.A.; and Snurr, R.Q. "Ultrahigh surface area zirconium MOFs and insights into the applicability of the BET theory." *J Am Chem Soc*, 2015. **137**(10):3585–3591. doi:10.1021/ja512973b
- (S20) Park, H.J. and Suh, M.P. "Mixed-Ligand Metal-Organic Frameworks with Large Pores: Gas Sorption Properties and Single-Crystal-to-Single-Crystal Transformation on Guest Exchange." *Chem Eur J*, 2008. **14**(29):8812–8821. doi:10.1002/chem.200801064
- (S21) Pillai, R.S.; Yoon, J.W.; Lee, S.J.; Hwang, Y.K.; Bae, Y.S.; Chang, J.S.; and Maurin, G. "N<sub>2</sub> Capture Performances of the Hybrid Porous MIL-101(Cr): From Prediction toward Experimental Testing." *J Phys Chem C*, 2017. **121**(40):22130–22138. doi:10.1021/acs.jpcc.7b07029